

Modeling ice-shelf cavities using Lagrangian elements

A.A. Stern,¹, A. Adcroft¹ and O. Sergienko¹, G. Marques¹, R. Hallberg¹

2 **Key Points:**

3

- 4 • A novel modeling framework is developed to model breakable ice shelves and ice-shelf cavities
5 using Lagrangian elements, held together by numerical bonds.
- 6 • The ocean circulation beneath a (static) Lagrangian ice shelf is almost indistinguishable
7 from the circulation beneath an Eulerian ice-shelf model run in an identical configuration.
- 8 • The similarity between the models provides a proof of concept for the Lagrangian model,
9 allowing the Lagrangian model to be used simulations involving tabular iceberg calving.

A. A. Stern, Geophysical Fluid Dynamics Laboratory, Princeton University

A. Adcroft, Geophysical Fluid Dynamics Laboratory, Princeton University

O. Sergienko, Geophysical Fluid Dynamics Laboratory, Princeton University

G. Marques, Geophysical Fluid Dynamics Laboratory, Princeton University

R. Hallberg, Geophysical Fluid Dynamics Laboratory, Princeton University

10 Abstract.

11 The calving of large tabular icebergs away from Antarctic ice shelves is an
12 important feature of the Antarctic environment, and accounts for approx-
13 imately half of Antarctic ice-shelf decay. However, despite its importance,
14 the current generation of ice-ocean models is unable to represent ice-shelf
15 calving in a physically realistic way. One reason for this is that current ice-
16 shelf models are mostly built on static Eulerian grids, and were not designed
17 to easily allow pieces of the ice shelf to break off and become icebergs. In this
18 study we develop a new ice-shelf cavity model where the ice shelf is constructed
19 out of Lagrangian elements that are bonded together by numerical bonds.

20 This Lagrangian framework allows for large pieces of the ice shelf to break
21 away and become tabular icebergs. We test newly developed Lagrangian ice
22 -shelf model by simulating the circulation within a (static) idealized ice-shelf
23 cavity, which was developed as part of the Marine Ice Ocean Modeling Inter-
24 comparison Project (MISOMIP). The Lagrangian model results are compared
25 to a second simulation that uses an Eulerian ice shelf with an otherwise iden-
26 tical configuration. Results show that the Lagrangian and Eulerian models
27 are almost indistinguishable. The similarly between the Eulerian and Lagrangian
28 models in a static ice-shelf configuration provides a proof of concept for the
29 Lagrangian model, and means that we can confidently use Lagrangian ice-
30 shelf models to extend the capabilities of the Eulerian models.

1. Introduction

31 Floating ice shelves cover vast regions of the Antarctic polar oceans. These massive
32 platforms of ice extend deep into the water column, applying large pressures to surface
33 of the ocean, which is often hundreds of meters below global sea level. Beneath the ice
34 shelves, both the bottom topography and the ice-shelf geometry play a role in steering
35 ocean currents [Nicholls , 1996; Jenkins et al , 2010; Stern et al , 2014]. The topographic
36 constraint imposed by the ice shelves at the ocean's upper boundary significantly affects
37 the circulation within the ice-shelf cavities, and gives the ocean in the region a unique
38 character.

39 Satellite observations suggest that ice-shelf decay occurs via two main processes: melting
40 and breaking [Depoorter et al , 2013; Rignot et al , 2013]. Each of these is responsible for
41 approximately half of the ice-shelf decay, and each influences the surrounding ocean (and
42 ice-shelf geometry) in a distinct way. Melting at the base of ice shelves causes freshwater
43 fluxes into the ice-shelf cavity. The input of buoyant meltwater creates rising density
44 plumes, which are guided along the ice-shelf base, and help drive ocean circulation beneath
45 the ice shelves [MacAyeal , 1984; Holland and Feltham , 2006]. Over time, melting at the
46 ice-shelf base can erode the ice shelf, gradually altering the ice-shelf geometry. In contrast,
47 ice-shelf breaking causes sudden changes to the ice-shelf geometry, and releases giant
48 icebergs into the ocean. After calving, these tabular icebergs can travel large distances
49 and impact ocean hydrography [Martin and Adcroft , 2010; Stern et al , 2015], sea-ice
50 formation [Robinson et al , 2012; Stern et al , 2016] and ocean biology [Smith et al , 2007;
51 Vernet et al , 2012; Biddle et al , 2015] many miles away.

52 In recent years society's need for improved projections of future sea level has lead to
53 an increased focus on the Antarctic mass balance, and hence, on modeling Antarctic sub-
54 ice-shelf cavities [Asay-Davis et al , 2016]. Modeling the ocean beneath the ice shelves
55 presents a unique set of challenges, since (i) the presence of ice shelves provides a rigid
56 upper boundary for the ocean model which is not encountered elsewhere in the ocean, and
57 (ii) melting and breaking ice shelves imply a changing ocean boundary conditions which
58 present numerous numerical difficulties.

59 The earliest models of ocean ice-shelf cavities were developed using static ice shelves
60 with a fixed shape [Hellmer and Olbers , 1989; Determan and Gerdes , 1994; Grosfeld et
61 al , 1997; Holland and Jenkins , 2001; Losch , 2008]. In these models, ice-shelf melting
62 was represented through salinity and temperature fluxes, while the ice-shelf geometry
63 remained unchanged. Later models of ice-shelf cavities allowed the ice-shelf geometry
64 to evolve as the ice shelf melted, permitting the study of coupled ocean-ice phenomena
65 [Gladish et al , 2012; Sergienko , 2013]. More recently, dynamic ice-shelf models have been
66 coupled the ocean cavity, allowing the study of grounding line migration, which is of key
67 importance for sea level rise projections [Grosfeld and Sandhger , 2004; Goldberg et al ,
68 2012; De Rydt and Gudmundsson , 2016].

69 As far as we know, all models of ice-shelf cavities to date have omitted ice-shelf breaking
70 and iceberg detachment. This is because (i) there is much uncertainty of the physics
71 that govern ice-shelf breaking [Benn et all , 2007; Alley et al , 2008; Levermann et al
72 , 2012; Bassis and Jacobs , 2013], and (ii) current models of ice-shelf cavities represent
73 the ice shelves on static Eulerian grids, which do not lend themselves to modeling iceberg
74 detachment and drift. In contrast, existing *iceberg* models represent icebergs as Lagrangian

75 particles, since this is a convenient way to model discrete objects traveling over large
76 distances [Bigg et al , 1997; Gladstone et al , 2001; Martin and Adcroft , 2010; Marsh et
77 al , 2015]. To date there has been no real effort to synthesize these two approaches (i.e.:
78 to combine ice shelf and iceberg models).

79 In this study we develop a new ice-shelf cavity model where the ice shelf is represented
80 on a ‘Lagrangian grid’. In this model, the ice shelf is constructed out of Lagrangian
81 elements which are bonded together by numerical bonds (see schematic Figures 1). This
82 Lagrangian framework allows for large pieces of the ice shelf to break away and become
83 tabular icebergs. An example of this enhanced capability of the Lagrangian model is
84 demonstrated in Figures 2, which shows a tabular iceberg drifting away an idealized ice
85 shelf (see Stern et al [2017] for more details).

86 However, before analyzing the improved capabilities of the Lagrangian ice-shelf model,
87 it is necessary to thoroughly test and benchmark the Lagrangian model in a more familiar
88 configuration. To do this we compare the Lagrangian ice-shelf-cavity model to existing Eu-
89 larian model in a static ice-shelf configuration. For this comparison, we use the model con-
90 figuration developed as part of the Marine Ice Ocean Modeling Inter-comparison Project
91 (MISOMIP). The goals of this study are (i) to introduce and describe the Lagrangian ice-
92 shelf model, and (ii) to prove that the Lagrangian model can replicate the behavior of an
93 Eularian ice-shelf model when modeling ocean cavities beneath static ice shelves. Demon-
94 strating that the Lagrangian model compares well to more traditional Eularian models
95 is a prerequisite for using the Lagrangian model to move beyond the capabilities of the
96 Eularian model, and increases our confidence in more complex Lagrangian simulations
97 involving calving icebergs.

2. Lagrangian model description

98 The Kinematic Iceberg Dynamics (KID) model is Lagrangian model that has been
99 developed in order to simulate ice-shelf cavities with breakable ice shelves. The model
100 represents ice shelves using Lagrangian elements joined together by numerical bonds. By
101 breaking these bonds, the model is able to simulate ice-shelf calving and iceberg breakup.

102 The goal of this study is to show that this Lagrangian ice-shelf model can replicate the
103 results of an Eulerian ice-shelf model when used in a static ice-shelf configuration (with
104 all the elements being held stationary). Although the ice elements do not move in the
105 static ice-shelf experiment, this configuration is a relevant test for the Lagrangian model,
106 as it tests the interpolation and aggregation between Eulerian and Lagrangian grids,
107 and also test the coupling between the ocean and ice-shelf models. Benchmarking the
108 Lagrangian ice-shelf model to an existing Eulerian model in a static ice-shelf configuration
109 is a prerequisite for using the Lagrangian model in more complex experimental setups with
110 moving elements.

111 In this section we briefly describe the fully dynamic Lagrangian ice-shelf model. We
112 then focus on element packing and interpolation between the Eulerian and Lagrangian
113 grids, which are the parts of the model which are relevant to static ice simulations. A
114 complete description of the KID model, including details of the momentum budget and
115 element interactions can be found in Stern et al [2017].

2.1. Kinematic Iceberg Dynamics model

116 The KID model is a Lagrangian particle-based model, in that the objects of the model
117 are Lagrangian elements. Each Lagrangian element represents a column of ice that is
118 floating in the ocean. The elements each have their own position, velocity, mass, and a

set of dimensions, which can evolve in time. Each element moves according to its own momentum equation which is solved in the (Lagrangian) reference frame of the element. The elements are forced by oceanic, sea ice and atmospheric drag forces, as well as a forces due to sea surface height gradients, and the Coriolis force [Bigg et al , 1997; Gladstone et al , 2001; Martin and Adcroft , 2010; Stern et al , 2017]. The elements also interact with other elements and can be ‘bonded’ together by numerical bonds, which hold the elements together and allow many elements to move together as a unit. By bonding many ice elements together, the model is able to form larger structures, such as tabular icebergs or ice shelves (see schematic Figures 1).

The Lagrangian elements melt when they are exposed to above-freezing ocean mixed-layer temperatures. The melt rates of the elements are prescribed using parametrizations developed for iceberg and ice-shelf decay [Bigg et al , 1997; Holland and Jenkins , 1999; Gladstone et al , 2001; Martin and Adcroft , 2010]. As the elements melt, heat, salt and mass fluxes are passed to the ocean to simulate freshwater injection to the ocean surface.

2.2. Initializing element geometry and packing

The elements in the Lagrangian model are assumed to have surface areas which are shaped as equally-sized regular hexagons. We initialize the Lagrangian model by positioning the elements in a staggered lattice, so that the elements fit together and perfectly tile the ice-shelf surface (Figures 1b). Hexagonal elements are used so that when adjacent pairs of elements are bonded together, the network of bonds form equilateral triangles, which gives rigidity to the larger structure [Stern et al , 2017].

2.3. Interpolation and aggregation onto the Lagrangian grid

When constructing ice shelves using the Lagrangian model, the collection of elements can be thought of as being a ‘Lagrangian grid’ for the ice shelf. In this framework the nodes of the Lagrangian grid (elements) can move at every time step, altering the shape of the ice shelf. This is in contrast to the more traditional approach of modeling ice shelves on an Eulerian grid, where the grid is fixed in time. Using a Lagrangian grid is a convenient framework for modeling breakable ice shelves since it allows pieces of the ice-shelf grid to break away from the ice shelf and become part of the iceberg grid [Stern et al , 2017].

In the experiments presented in this study, the ice-shelf model is coupled to an ocean model, which runs on a static Eulerian grid. At every time step, ice-shelf fields are passed from the ice-shelf model to the ocean model and from the ocean model to the ice-shelf model. Four ocean (mixed layer) fields are passed from the ocean model to the ice-shelf model: temperature, salinity and zonal and meridional velocities. These fields are interpolated onto the Lagrangian grid (i.e.: onto the elements in the ice-shelf model) using a bilinear interpolation scheme.

At the end of a ice-shelf model time step, ice-shelf fields are aggregated from the elements back onto the Eulerian ocean grid, and are then passed from the ice-shelf model to the ocean model. The aggregation from the Lagrangian grid to the Eulerian ocean grid is done in a way which is consistent with the shape of the elements. For the purposes of aggregation, we assume that the elements have surface areas that are shaped as regular hexagons. Element’s properties are aggregated from the Lagrangian grid to the Eulerian grid by exactly calculating fraction of an elements surface area that is contained in

¹⁶¹ each ocean grid cell, and dividing the element's properties between the ocean grid cell in
¹⁶² proportion to that fraction.

2.4. Lagrangian vs Eularian ice-shelf model

¹⁶³ In the next section, simulations using the Lagrangian ice-shelf model are compared to
¹⁶⁴ simulations using an Eularian ice-shelf model with an an identical configuration. While
¹⁶⁵ the internal framework and grids of the Eularian and Lagrangian ice-shelf models are
¹⁶⁶ quite different, both models are coupled to the ocean model using the same coupling
¹⁶⁷ structure. Five fields are passed from the ice-shelf models to ocean model: mass, surface
¹⁶⁸ area, temperature flux, salinity flux and mass flux. The Eularian model uses the same
¹⁶⁹ grid as the ocean model, while in the Lagrangian model these fields are aggregated onto
¹⁷⁰ the ocean model grid before being passed through the coupler. Once in the ocean model,
¹⁷¹ these fields and are used to: (i) apply a pressure to the ocean surface, (ii) alter the upper-
¹⁷² ocean boundary condition to reflect that the ocean is covered by ice, and (iii) apply salt,
¹⁷³ temperature and mass fluxes associated with ice-shelf melting and freezing.

¹⁷⁴ Since the coupling with the ocean model is handled in the same way for both the
¹⁷⁵ Eularian and Lagrangian models and both models are coupled to the same ocean model,
¹⁷⁶ any differences between the two models in the static ice-shelf configuration (using the same
¹⁷⁷ melt rate parametrization) are likely due to the interpolation/aggregation between the ice
¹⁷⁸ and ocean grids. By accurately aggregating fields from the Lagrangian grid to Eularian
¹⁷⁹ ocean grids, we can make the Lagrangian ice-shelf model behave like the Eularian ice-shelf
¹⁸⁰ model in static ice-shelf simulations.

3. Experiment Setup

181 The KID model is used to simulate the flow within an idealized ice-shelf cavity. The
 182 simulations are repeated using an Eulerian ice shelf with an identical configuration. The
 183 details of the experimental setup for both the Lagrangian and Eulerian models are pre-
 184 sented here.

3.1. Domain configuration

185 In order for our simulations to be easily comparable to previous models of ice-shelf
 186 cavities, we use an experimental setup based on the configuration created for the Marine
 187 Ice Ocean Modeling Inter-comparison Project (MISOMIP) [Asay-Davis et al , 2016]. The
 188 MISOMIP configuration was developed as a standardized configuration to allow for a
 189 comparison between various ocean-ice coupled models. The configuration consists of an
 190 idealized ice shelf in a rectangular domain $L_x = 80\text{km}$ long and $L_y = 480\text{km}$ wide.
 191 The ice shelf is grounded on the southern side of the domain with the ice-shelf front at
 192 $y=650\text{km}$. The ice thickness and bottom topography of this setup are shown in Figure 3.
 193 The configuration is the same as that of the Ocean0 setup in the MISOMIP, with three
 194 changes made:

- 195 1. The ‘calving criteria’ used in the MISOMIP study (which states that all points in
 196 the ice shelf with thickness less than 100m are set to zero thickness) has not been used.
- 197 2. The ice shelf has been thickened on the flanks of the domain, so that the latitude of
 198 the grounding line increases away from the center of the ice shelf.
- 199 3. The ice shelf is configured to be symmetric about its meridional center line ($x = \frac{L_x}{2}$).
 200 This was achieved by using the average of the left and right flanks of the ice-shelf thickness.

201 These three changes were made in order to make the circulation beneath the ice shelf
202 easier to interpret.

3.2. Ocean Model

203 The Lagrangian and Eulerian ice shelves are coupled to the MOM6 ocean model [Hall-
204 berg et al , 2013]. The ocean model is run in using vertical coordinate system which is
205 a hybrid between a sigma-level and a z-level coordinate, achieved using ALE regridding-
206 remapping scheme [White et al , 2009]. In this vertical coordinate, model layers bend
207 underneath surface topography (i.e.: the ice shelf), as they would in a sigma coordinate
208 model, and intersect the bottom topography, as they would in a z-coordinate model. The
209 model has 72 vertical layers and has a horizontal resolution of $\Delta x = 2$ km. The numerical
210 simulations were all repeated using an isopycnal coordinate (without ALE regrinding-
211 remapping). The results were qualitatively similar to the ALE results, and are therefore
212 not presented here.

213 The ocean parameters used in the simulations are as specified in the MISOMIP config-
214 uration [Asay-Davis et al , 2016], and are shown in Table 1. The simulation is initialized
215 from rest, with horizontally uniform initial ocean temperature and salinity profiles which
216 vary linearly between specified surface and bottom values: $T_{top} = -1.9^{\circ}\text{C}$, $T_{bottom} = 1.0^{\circ}\text{C}$,
217 $S_{top} = 33.8$ psu, $S_{bottom} = 34.7$. The maximum ocean depth is $H_{ocean} = 720$ m. A sponge
218 layer is used on the northern boundary, which relaxes back to the initial temperature
219 and salinity with a relaxation time scale of $T_{sponge} = 0.1$ days over a distance of 10 km.
220 Melting is set to zero for ocean cells where the ocean column thickness is less than 10m.

3.3. Lagrangian ice-shelf simulations:

The Lagrangian ice shelf is created using 10882 Lagrangian hexagonal elements with sides of length $S = 0.98$ km . The positions of the hexagonal elements are initialized by packing them together in a space-filling staggered lattice. Gaps along the boundaries are filled in using smaller elements so that the total ice-shelf area is preserved. The initial mass of the ice elements is determined by a preprocessing inversion step, which is the inverse of the aggregation procedure discussed in Section 2.3.

3.4. Eularian ice-shelf simulations:

The Eularian ice-shelf simulation is performed using an existing Eulerian ice-shelf cavity model [Goldberg et al , 2012], which is an optional module of the the MOM6 ocean model. The ice shelf is initialized on the same grid as the ocean model with a horizontal resolution of $\Delta x = 2$ km. The ice-shelf thickness field is initialized using the same ice-shelf draft used for the Lagrangian model (Figure 3).

3.5. Ice-shelf decay

The melt rates in both the Lagrangian and Eularian ice-shelf simulations are calculated using the 3 equation model for ice-shelf decay [Holland and Jenkins , 1999]. In both experiments the ice shelf is held stationary. In the Eularian code, this is achieved by setting the ice-shelf velocity to zero, while in Lagrangian ice shelf, the element velocities are set to zero. In both simulations, the ice shelf is thermodynamically active and is able to ‘melt’ but has a constant thickness (as specified in the Ocean0 experiment in the MISOMIP [Asay-Davis et al , 2016]). In this setup, ice-shelf melting generates temperature and salinity fluxes into the ocean, but does not change the thickness of the ice shelf / ice

elements. This can be thought to represent an ice shelf in dynamic equilibrium where the melt is exactly balanced ice-shelf advection.

4. Results

4.1. Results from the Lagrangian ice-shelf simulation

The results from the Lagrangian ice-shelf simulation fit within the current understanding of ice-shelf cavity circulations based on ice-shelf observations [MacAyeal , 1984; Lewis and Perkin , 1986; Jacobs et al , 2011] and previous modeling efforts [Determan and Gerdes , 1994; Holland and Feltham , 2006; Losch , 2008]. The ocean temperatures inside the domain are warmer than the in-situ freezing point (Figure 4a), and cause melting at the ice-shelf base (Figure 5c). The meltwater entering the domain is more buoyant than the water around it, and rises along the ice shelf as a cool fresh plume (Figure 4). This injection of positive buoyancy at depth drives a clockwise circulation outside of the ice-shelf cavity (Figure 6a), providing the ice-shelf cavity with a continuous supply of warm water, which provides the thermal energy required for continuous ice-shelf melt.

The highest melt rates are observed within 100km of the grounding line (Figure 5a). These elevated melt rates are caused by the presence of warm water (Figure 5d) and increased ocean velocities (Figure 5c) near the grounding line, as well as the fact that freezing point of ice decreases with increasing pressure. Elevated melt rates are also seen near the ice front, caused by strong currents running along the ice-shelf front (Figure 5c).

4.2. Comparison of Lagrangian and Eulerian ice-shelf models

The Lagrangian ice-shelf model results are qualitatively similar to most of the simulations from the MISOMIP experiment [Asay-Davis et al , 2016], which use a similar

259 configuration (see Section 3.4). To get a quantitative comparison, we compare the La-
260 grangian ice-shelf model results to a simulation using an Eulerian ice-shelf model with an
261 identical configuration. The results show that two simulations are almost indistinguish-
262 able. This is demonstrated, for example, in Figures 6, which shows the time-averaged
263 barotropic stream function of the Lagrangian (Figures 6a) and Eulerian (Figures 6b)
264 simulations, and the difference between the two (Figures 6c). The difference between
265 the Lagrangian and Eulerian barotropic stream functions are two orders of magnitude
266 smaller than typical differences observed between simulations using different models in
267 the MISOMIP [Asay-Davis et al , 2016]. The similarity of the Lagrangian and Eulerian
268 simulations are also reflected in the fact that the simulations have very similar ice-shelf
269 melt rates and ocean temperature/salinity profiles (shown in Figures S1 and Figures S2
270 in the supplementary materials).

271 The agreement between the Eulerian and Lagrangian simulations is a confirmation that
272 the Lagrangian model is able to simulate sub-ice-shelf cavities as well as the Eulerian
273 model does. This is a good starting point for moving beyond the capabilities of the
274 Eulerian model.

5. Conclusion

275 This study presents a new Lagrangian framework for modeling sub-ice-shelf cavities.
276 In this framework, the ice shelf is constructed out of many Lagrangian elements, which
277 are bonded together by numerical bonds. The collection of Lagrangian elements can
278 be thought of as being a Lagrangian grid, which stores the ice-shelf properties. Unlike
279 Eulerian grids, the nodes (elements) can move at every time step, altering the shape of
280 the ice shelf. This allows us to use the Lagrangian ice-shelf model to large pieces of the

ice-shelf breaking away from the ice shelf to becoming tabular icebergs that are fully embedded in the ocean (Figures 2). This capability is currently not possible using more traditional Eulerian models [Stern et al , 2017].

The present study focuses on using the Lagrangian ice shelf to model static ice shelves. The model is demonstrated by modeling the circulation beneath a (static) idealized ice shelf, which was developed as part of the MISOMIP inter-comparison project. The results from the Lagrangian ice-shelf model fit within our paradigm of understanding for circulation within ice-shelf cavities: buoyant meltwater that enters the ice-shelf cavity drives freshwater plumes at the ice-shelf base, which drives the circulation within the cavity. The circulation, melt rates and ocean hydrography achieved using the Lagrangian ice shelf compare well with other simulations in the MISOMIP experiments.

A direct comparison comparison between the Lagrangian and a Eulerian ice-shelf model coupled to the same ocean model shows that the results are extremely similar. Differences between the Lagrangian and Eulerian ice shelves models (resulting from interpolation errors) are much smaller than the differences observed when changing the ocean vertical coordinate system (for example). Demonstrating that the Lagrangian ice-shelf model is able to reproduce the results of an Eulerian ice-shelf model in the same static ice-shelf configuration is a prerequisite developing more advanced Lagrangian ice-shelf models and represents a good benchmark test for new Lagrangian ice-shelf models.

References

- 300 Asay-Davis, X. S., S. L. Cornford, B. K. Galton-Fenzi, R. M. Gladstone, G. H. Gudmundsson, D. M. Holland, P. R. Holland, and D. F. Martin (2016), Experimental design for
301 three interrelated marine ice sheet and ocean model intercomparison projects: MIS-
302 MIP v. 3 (MISMIP+), ISOMIP v. 2 (ISOMIP+) and MISOMIP v. 1 (MISOMIP1).
303 *Geoscientific Model Development* 9, no. 7: 2471.
- 304 Arrigo, K. R., G. L. van Dijken, D. G. Ainley, M. A. Fahnestock, and T. Markus (2002).
305 Ecological impact of a large Antarctic iceberg. *Geophys. Res. Lett.*, 29(7).
- 306 Alley, R. B., H. J. Horgan, I. Joughin, K. M. Cuffey, T. K. Dupont, B. R. Parizek, S.
307 Anandakrishnan, and J. Bassis (2008), A simple law for ice-shelf calving. *Science* 322,
308 no. 5906, 1344-1344.
- 309 Bassis, J. N., and S. Jacobs (2013), Diverse calving patterns linked to glacier geometry.
310 *Nature Geoscience*, 6(10), 833-836.
- 311 Benn, D. I., C. R. Warren, and R. H. Mottram (2007). Calving processes and the dynamics
312 of calving glaciers. *Earth-Science Reviews*, 82(3), 143-179.
- 313 Bigg, G. R., Wadley, M. R., Stevens, D. P., and Johnson, J. A. (1997), Modeling the
314 dynamics and thermodynamics of icebergs. *Cold Regions Science and Technology*, 26(2),
315 113-135.
- 316 Borstad, C. P., A. Khazendar, E. Larour, M. Morlighem, E. Rignot, M. P. Schodlok, and
317 H. Seroussi (2012), A damage mechanics assessment of the Larsen B ice shelf prior to
318 collapse: Toward a physically-based calving law, *Geophys. Res. Lett.*, 39, L18502
- 319 Biddle, L. C., J. Kaiser, K. J. Heywood, A. F. Thompson and A. Jenkins (2015), Ocean
320 glider observations of iceberg-enhanced biological productivity in the northwestern Wed-

- 322 dell Sea, *Geophys. Res. Lett.*, 42, 459465.
- 323 De Rydt, J., and G. H. Gudmundsson (2016), Coupled ice shelf ocean modeling and
324 complex grounding line retreat from a seabed ridge. *J. of Geophys. Res.: Earth Surface*,
325 121(5), 865-880.
- 326 Dunne, J.P., J.G. John,, A.J. Adcroft, S.M. Griffies, R.W. Hallberg, E. Shevliakova,
327 R.J. Stouffer, W. Cooke, K.A. Dunne, M.J Harrison, and J.P. Krasting (2012), GFDL's
328 ESM2 global coupled climate-carbon Earth System Models. Part I: Physical formulation
329 and baseline simulation characteristics. *J. of Climate*, 25(19), 6646-6665.
- 330 Depoorter, M. A., J. L. Bamber, J. A. Griggs, J. T. M. Lenaerts, Stefan RM Ligtenberg,
331 M. R. van den Broek, and G. Moholdt (2013), Calving fluxes and basal melt rates of
332 Antarctic ice shelves. *Nature*, 502(7469), 89-92.
- 333 Determan J., Gerdes R. (1994), Melting and freezing beneath ice shelves: implications
334 from a three-dimensional ocean-circulation model. *Ann. Glaciol.*, 20, 413-419.
- 335 Dowdeswell, J. A., and J. L. Bamber (2007), Keel depths of modern Antarctic icebergs
336 and implications for sea-floor scouring in the geological record. *Marine Geology*, 243(1),
337 120-131.
- 338 Duprat, L. P., G. R. Bigg, and D. J. Wilton (2016), Enhanced Southern Ocean marine
339 productivity due to fertilization by giant icebergs. *Nature Geoscience*.
- 340 Eckert, E. R. G. (1950). Introduction to the Transfer of Heat and Mass. McGraw-Hill.
- 341 Gladstone, R. M., G. R. Bigg, and K. W. Nicholls. (2001), Iceberg trajectory modeling
342 and meltwater injection in the Southern Ocean (19782012). *J. of Geophys. Res.: Oceans*,
343 106(C9), 19903-19915.

- ³⁴⁴ Goldberg, D. N., C. M. Little, O. V. Sergienko, A. Gnanadesikan, R. Hallberg, and M.
³⁴⁵ Oppenheimer (2012), Investigation of land ice?ocean interaction with a fully coupled
³⁴⁶ ice-ocean model: 1. Model description and behavior. *J. of Geophys. Res.: Earth Surface*,
³⁴⁷ 117(F2).
- ³⁴⁸ Gladish, C. V., D. M. Holland, P. R. Holland, and S. F. Price (2012), Ice-shelf basal
³⁴⁹ channels in a coupled ice/ocean model. *J. of Glaciol.*, 58(212), 1227-1244.
- ³⁵⁰ Grosfeld K., R. Gerdes, J. Determan (1997), Thermohaline circulation and interaction
³⁵¹ between ice shelf cavities and the adjacent open ocean. *J. Phys. Oceanogr.*, **102**, C7,
³⁵² 15959-15610.
- ³⁵³ Grosfeld, K., and H. Sandhger, (2004). The evolution of a coupled ice shelfocean system
³⁵⁴ under different climate states. *Global and Planetary Change*, 42(1), 107-132.
- ³⁵⁵ Hallberg, R., A. Adcroft, J. P. Dunne, J. P., Krasting, R. J., and Stouffer (2013), Sensitiv-
³⁵⁶ ity of twenty-first-century global-mean steric sea level rise to ocean model formulation.
³⁵⁷ *J. of Climate*, 26(9), 2947-2956.
- ³⁵⁸ Holland D. M., Jenkins A. (2001), Adaptation of an isopycnic coordinate ocean model for
³⁵⁹ the study of circulation beneath ice shelves. *Mon. Wea. Rev.*, 129, 1905-1927.
- ³⁶⁰ Holland P. R. and D. L. Feltham (2006), The effects of rotation and ice shelf topography
³⁶¹ on frazil-laden Ice Shelf Water plumes. *J. Phys. Oceanogr.*, 36, 2312-2327.
- ³⁶² Holland, D. M., and A. Jenkins (1999), Modeling thermodynamic ice-ocean interactions
³⁶³ at the base of an ice shelf. *J. of Phys. Oceanogr.* 29.8, 1787-1800.
- ³⁶⁴ Hellmer H.H., Olbers D. J. (1989), A two-dimensional model for the thermohaline circu-
³⁶⁵ lation under an ice shelf. *Antarctic Science*, 1, 325- 336.

- ³⁶⁶ Hopkins, M. A. (1996). On the mesoscale interaction of lead ice and floes. *J. of Geophys. Res.: Oceans*, 101(C8), 18315-18326.
- ³⁶⁸ Jakobsen, T. (2001). Advanced character physics. In *Game Developers Conference*, Vol. 3.
- ³⁷⁰ Jenkins, A., P. Dutrieux, S. S. Jacobs, S. D. McPhail, J. R. Perrett, A. T. Webb, and D. White (2010), Observations beneath Pine Island Glacier in West Antarctica and implications for its retreat. *it Nature Geo.*, 3(7), 468-472.
- ³⁷³ Jacobs, S. S., A. Jenkins, C. F. Giulivi, and P. Dutrieux (2011). Stronger ocean circulation and increased melting under Pine Island Glacier ice shelf. *Nature Geo.*, 4(8), 519-523.
- ³⁷⁵ Jongma, J. I., E. Driesschaert, T. Fichefet, H. Goosse, and H. Renssen (2009), The effect of dynamic-thermodynamic icebergs on the Southern Ocean climate in a three-dimensional model, *Ocean Modell.*, 26, 104113.
- ³⁷⁸ Lewis E.L. and R.G. Perkin (1986), Ice pumps and their rates. *J. of Geophys. Res.*, 91, 11756-11762.
- ³⁸⁰ Losch, M. (2008). Modeling ice shelf cavities in az coordinate ocean general circulation model. *J. of Geophys. Res.: Oceans*, 113(C8).
- ³⁸² Li, B., H. Li, Y. Liu, A. Wang and S. Ji (2014), A modified discrete element model for sea ice dynamics. *Acta Oceanologica Sinica*, 33(1), 56-63.
- ³⁸⁴ Liu, M. B. and G. R. Liu (2010), Smoothed particle hydrodynamics (SPH): an overview and recent developments. *Archives of computational methods in engineering*, 17(1), 25-76.
- ³⁸⁷ Lichy, C., and H. H. Hellmer (2001). Modeling giant-iceberg drift under the influence of sea ice in the Weddell Sea, Antarctica. *J. of Glaciol.*, 47(158), 452-460.

- 389 Levermann, A., T. Albrecht, R. Winkelmann, M. A. Martin, M. Haseloff, and I. Joughin.
390 (2012), Kinematic first-order calving law implies potential for abrupt ice-shelf retreat.
391 *The Cryosphere*, 6(2), 273-286.
- 392 Martin, T., and Adcroft, A. (2010), Parameterizing the fresh-water flux from land ice
393 to ocean with interactive icebergs in a coupled climate model. *Ocean Modelling*, 34(3),
394 111-124.
- 395 Marsh, R., V. O. Ivchenko, N. Skliris, S. Alderson, G. R. Bigg, G. Madec, A. T. Blaker
396 Y. Aksenov, B. Sinha, A.C. Coward, and J.L. Sommer (2015), NEMOICB (v1. 0):
397 interactive icebergs in the NEMO ocean model globally configured at eddy-permitting
398 resolution. *Geoscientific Model Development* 8, no. 5 (2015): 1547-1562.
- 399 MacAyeal D.R. (1984), Thermohaline Circulation Below the Ross Ice Shelf: A Conse-
400 quence of Tidally Induced Vertical Mixing and Basal Melting. *J. Geophys. Res.*, 89,
401 597-606
- 402 Nicholls K.W. (1996), Temperature variability beneath Ronne Ice Shelf, Antarctica, from
403 thermistor cables. *J. Phys. Oceanogr.*, 11, 1199-1210.
- 404 Nicholls KW, Østerhus S, Makinson K (2009), Ice-Ocean processes over the continental
405 shelf of the southern Weddell Sea, Antarctica: a review. *Rev. Geophys.* 47(3).
- 406 Omelyan, I. P., M. I. Mryglod, and R. Folk (2002), Optimized Verlet-like algorithms for
407 molecular dynamics simulations. *Physical Review E*, 65(5), 056706.
- 408 Rignot, E., S. Jacobs, J. Mouginot, and B. Scheuchl (2013), Ice-shelf melting around
409 Antarctica. *Science*, 341, no. 6143 (2013): 266-270.
- 410 Robinson, N. J., M. J. M. Williams, P. J. Barrett, and A. R. Pyne (2010), Observations of
411 flow and ice-ocean interaction beneath the McMurdo Ice Shelf, Antarctica, *J. Geophys.*

- 412 *Res.*, 115, C03025
- 413 Pan, W., A. M. Tartakovsky, and J. J. Monaghan (2013). Smoothed particle hydrody-
414 namics non-Newtonian model for ice-sheet and ice-shelf dynamics. *J. of Comp. Phys.*,
415 242, 828-842.
- 416 Pralong, A., and M. Funk (2005), Dynamic damage model of crevasse opening and appli-
417 cation to glacier calving, *J. Geophys. Res.*, 110, B01309.
- 418 Sergienko, O. V. (2013). Basal channels on ice shelves. *J. of Geophys. Res.: Earth Surface*,
419 118(3), 1342-1355.
- 420 Silva, T. A. M., Bigg, G. R., and Nicholls, K. W. (2006), Contribution of giant icebergs
421 to the Southern Ocean freshwater flux. *J. of Geophys. Res.: Oceans*, 111(C3).
- 422 Smith, K., B. Robison, J. Helly, R. Kaufmann, H. Ruhl, H., T. Shaw, and M. Vernet
423 (2007), Free-drifting icebergs: Hotspots of chemical and biological enrichment in the
424 Weddell Sea, *Science*, 317, 478482.
- 425 Stern, A. A., D. M. Holland, P. R. Holland, A. Jenkins and J. Sommeria (2014), The effect
426 of geometry on ice shelf ocean cavity ventilation: a laboratory experiment. *Experiments*
427 in *Fluids*, 55(5), 1-19.
- 428 Stern, A.A., Johnson, E., Holland, D.M., Wagner, T.J., Wadhams, P., Bates, R., Abra-
429 hamsen, E.P., Nicholls, K.W., Crawford, A., Gagnon, J. and Tremblay, J.E. (2015),
430 Wind-driven upwelling around grounded tabular icebergs. *J. of Geophys. Res.: Oceans*,
431 120(8), 5820-5835.
- 432 Stern, A. A., A. Adcroft, and O. Sergienko (2016), The effects of Antarctic iceberg calv-
433 ing?size distribution in a global climate model. *J. of Geophys. Res.: Oceans*, 121(8),
434 5773-5788.

- 435 Stern, A. A., A. Adcroft, O. Sergienko, G. Marques, R. Hallberg (2017), Modeling tabular
436 icebergs coupled to an ocean model. *Ocean Modeling*
- 437 Swope, W. C., H. C. Andersen, P. H. Berens, and K. R. Wilson (1982), A computer
438 simulation method for the calculation of equilibrium constants for the formation of
439 physical clusters of molecules: Application to small water clusters. *The Journal of
440 Chemical Physics* 76, no. 1, 637-649.
- 441 Tournadre, J., N. Bouhier, F. Girard-Ardhuin, and F. Rmy (2016), Antarctic icebergs
442 distributions 1992-2014. *J. Geophys Res: Oceans*.
- 443 Vernet, M., et al. (2012), Islands of ice: Influence of free-drifting Antarctic icebergs on
444 pelagic marine ecosystems, *Oceanography*, 25(3), 3839
- 445 Weeks, W. F., and W. J. Campbell (1973). Icebergs as a fresh-water source: an appraisal.
446 *J. of Glaciol.*, 12(65), 207-233.
- 447 White, L., A. Adcroft, and R. Hallberg (2009), High-order regriddingremapping schemes
448 for continuous isopycnal and generalized coordinates in ocean models. *J. of Comp.
449 Phys.*, 228(23), 8665-8692.

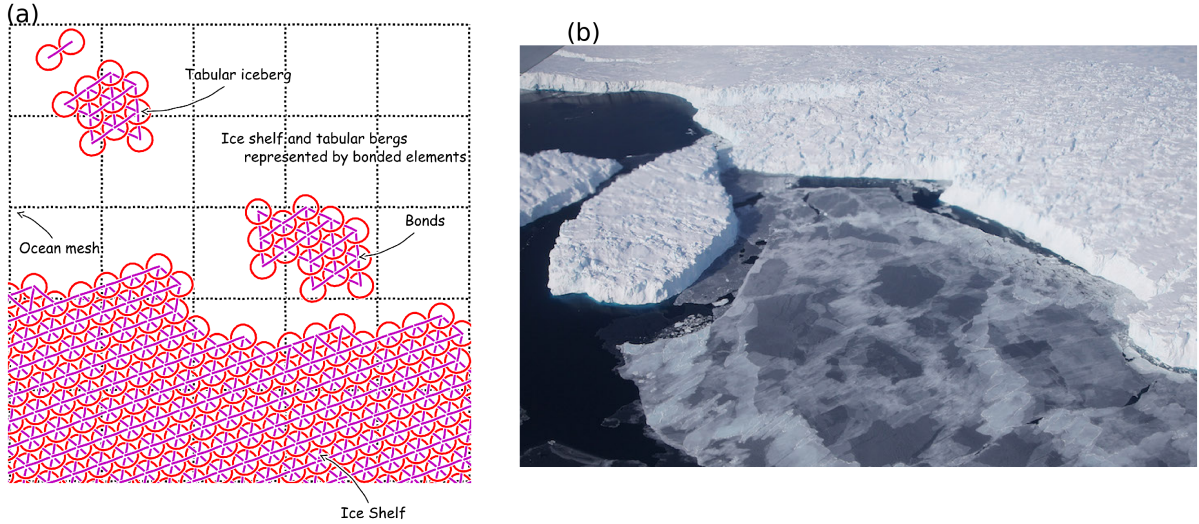


Figure 1. Schematic showing how ice shelves and tabular icebergs are constructed using Lagrangian elements. (a) Schematic of multiple ice elements that are joined together by numerical bonds (magenta lines) to form larger structures such as ice shelves and tabular icebergs. These numerical elements have finite extent and are able to interact with the ocean across multiple grid cells, and can interact with other elements. (b) Areal photograph of an ice shelf and tabular iceberg with elements superimposed over it to illustrate how the Lagrangian elements can be used to model ice shelves and tabular icebergs. In this schematic the ice elements (purple dots) are initialized in a staggered lattice covering the surface area of the iceberg. For purposes of mass aggregation, the ice elements are assumed to have hexagonal shape (red hexagons). For purposes of element interactions, the ice elements are assumed to be circular (black circles). Elements are initially bonded to adjacent elements using numerical bonds (magenta lines). These numerical bonds form equilateral triangles which give the shape rigidity. An ocean grid has been included (dashed cyan lines).

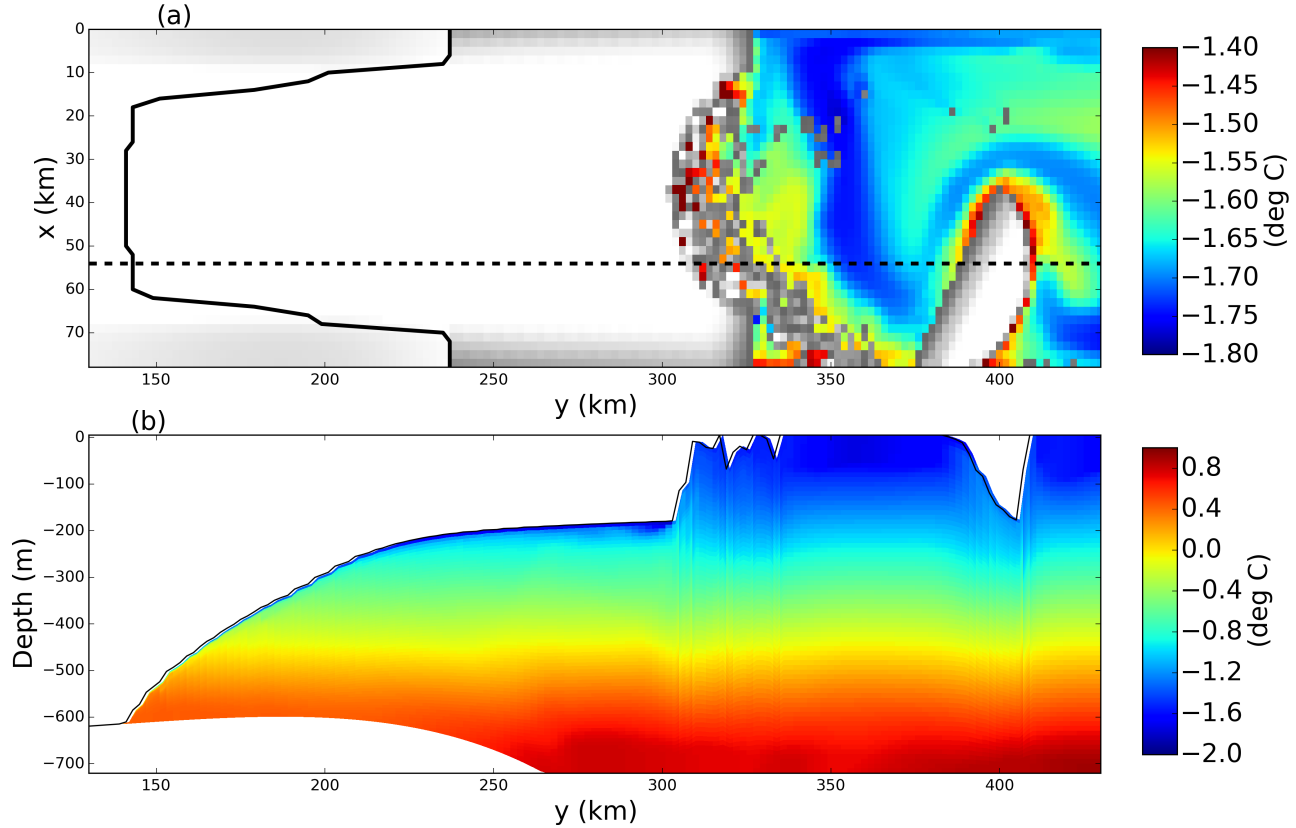


Figure 2. Snapshots of a simulation where a Lagrangian ice-shelf calves a tabular iceberg viewed (a) from above and (b) from the side. The snapshots are taken 30 days after calving. Panel (a) shows the sea surface temperature. Grid cells with ice mass $> 10^4$ kg are plotted in white, with grey shading indicating thinner ice. Panel (b) shows a vertical section of ocean temperature at $x=54$ km. The position of the vertical section is shown by the dashed line in panel (a). The solid line in panel (a) shows the position of the grounding line.

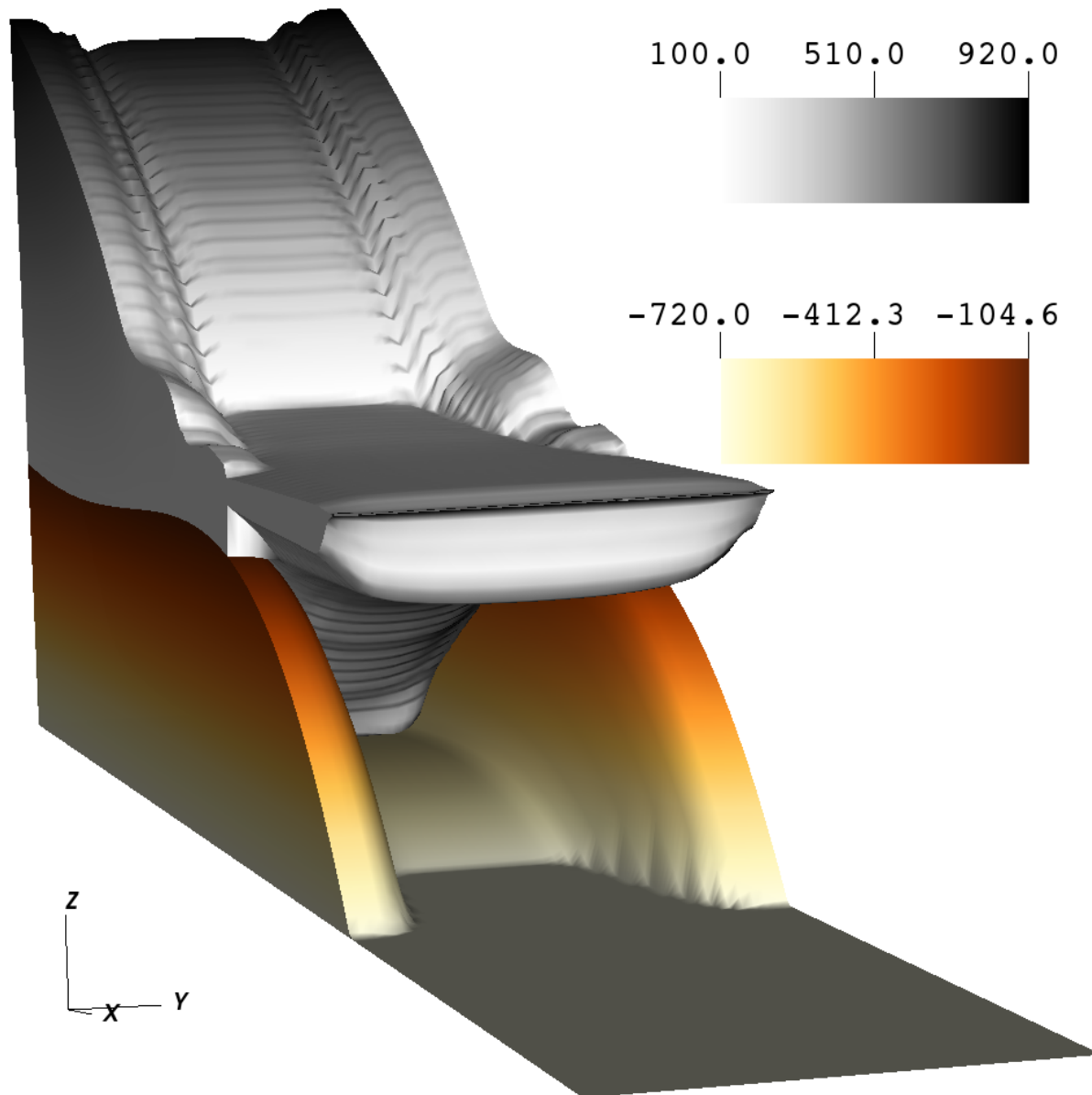


Figure 3. Ocean bottom topography and ice-shelf draft used in the Lagrangian and Eulerian static ice-shelf simulations

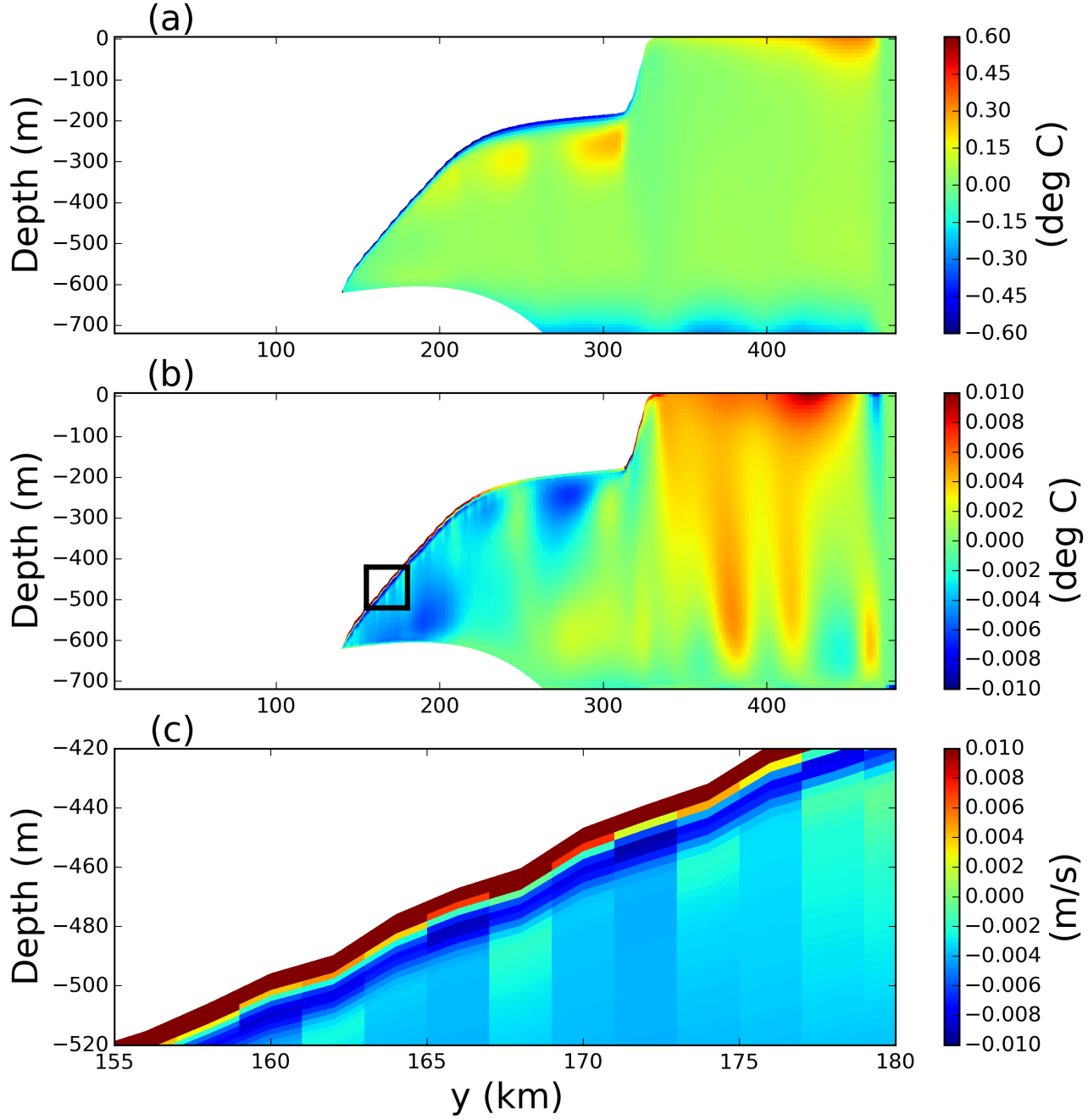


Figure 4. Snapshots of the static ice-shelf experiment taken after 5 years of model simulation, using the Lagrangian ice-shelf model coupled to the MOM6 ocean model. Panels show cross sections of the (a) ocean temperature anomaly relative to the initial temperature, and (b) the meridional ocean velocity. Panel (c) again shows the meridional ocean velocity, and is zoomed into the region near the ice-shelf base (the zoomed-in region is indicated with a black box (b)).

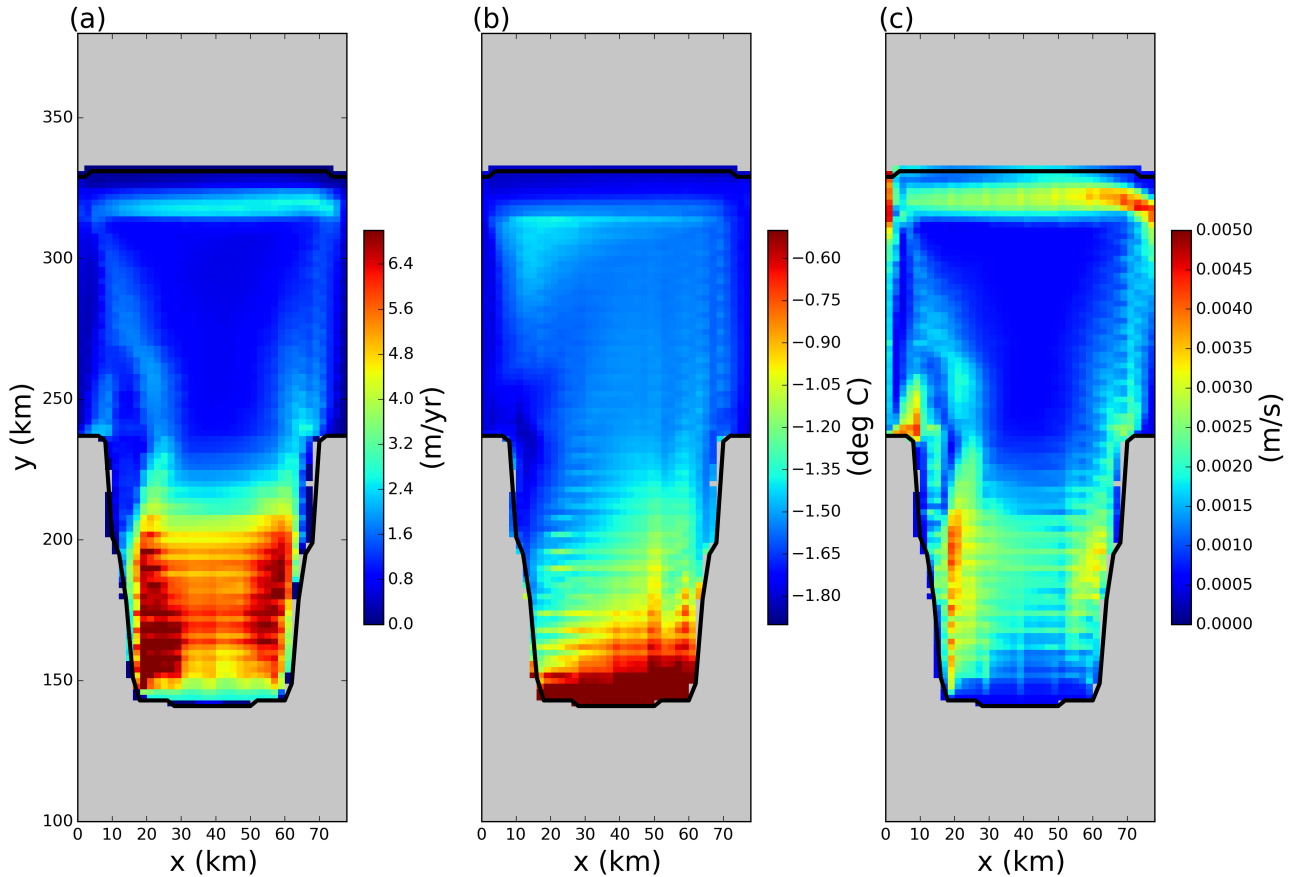


Figure 5. Results of the static ice-shelf experiment using the Lagrangian ice-shelf model coupled to MOM6. The three panels show 5 year time average of the (a) melt rate, (b) top-of-ocean temperature and (c) frictional velocity, u^* , at the base of the ice shelf. Fields are only shown in regions where the ice area fraction is ≥ 0.8 .

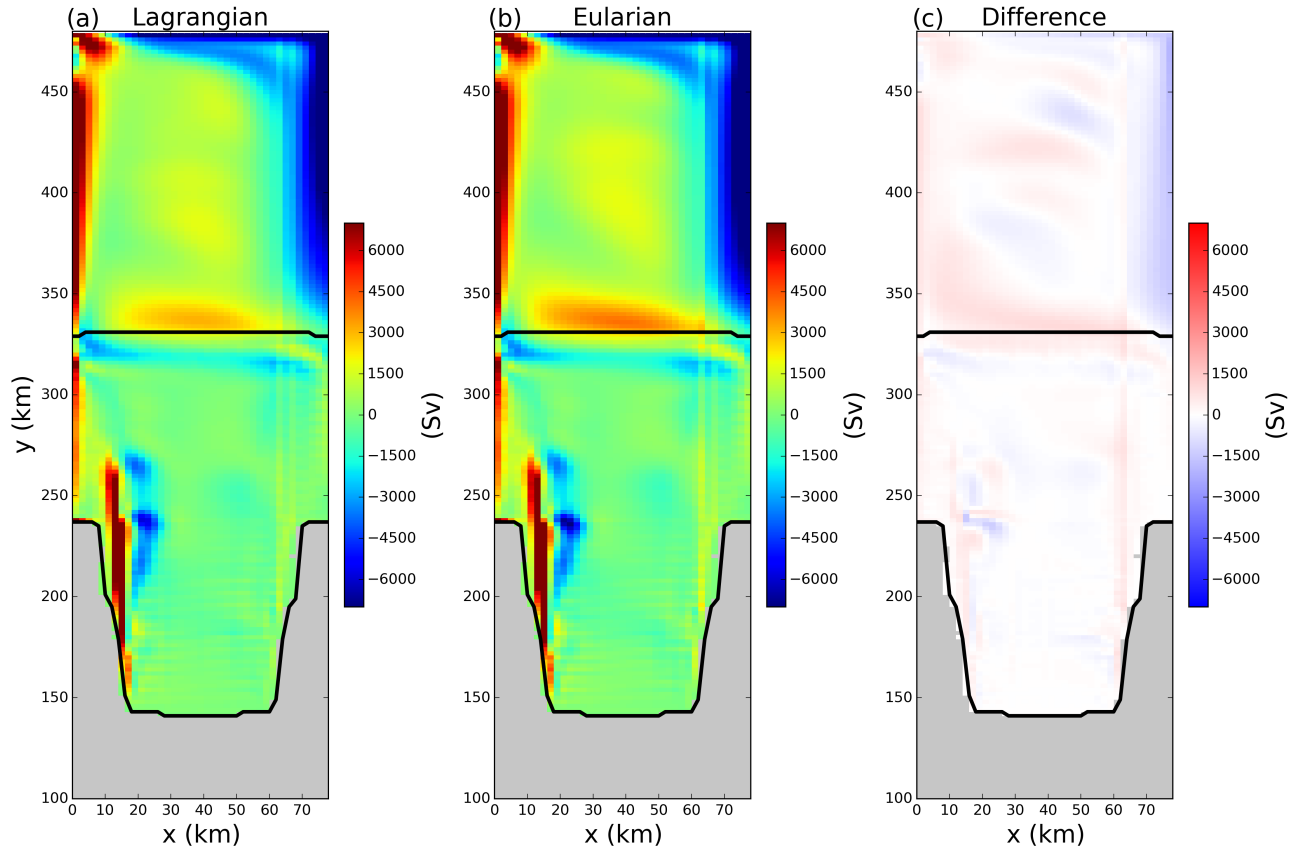


Figure 6. Time-averaged barotropic stream function in the (a) Lagrangian and (b) Eulerian simulations in the static ice-shelf configuration. Panel (c) shows the difference between panels (a) and (b). The time averages are taken over 5 years of model time, beginning at the end of the 5 year spin up period.

Parameter	Symbol	Value	Unit
Domain Length	L_x	80	km
Domain Width	L_y	480	km
Horizontal Resolution	Δx	2	km
Number of vertical layers	N_l	72	non-dim
Horizontal Viscosity	ν_H	6.0	$\frac{m^2}{s}$
Diapycnal Viscosity	ν_V	10^{-3}	$\frac{m^2}{s}$
Horizontal Diffusivity	ϵ_H	1.0	$\frac{s}{m^2}$
Diapycnal Diffusivity	ϵ_V	5×10^{-5}	$\frac{s}{m^2}$
Initial Surface Temperature	T_t	-1.9	$^{\circ}C$
Initial Bottom Temperature	T_b	1.0	$^{\circ}C$
Initial Surface Salinity	S_t	33.8	psu
Initial Bottom Salinity	S_b	34.7	psu
Maximum Ocean depth	H_{ocean}	720	m
Relaxation Time of Sponge Layer	T_{sponge}	0.1	days
Time Step for Static Shelf Experiment	dt_{Static}	1000	s
Time Step for Iceberg Calving Experiment	$dt_{Calving}$	10	s

6. Supplementary Figures

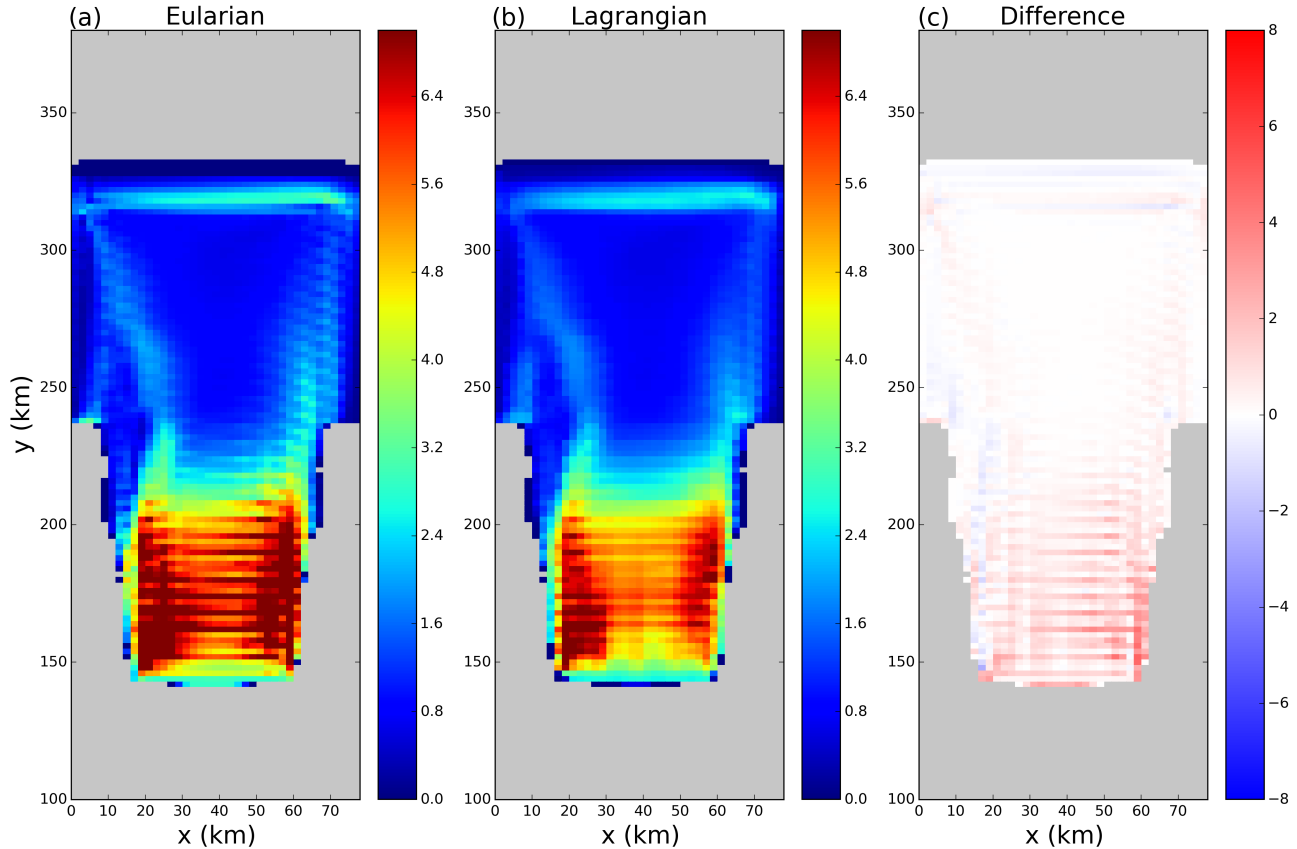


Figure S1. Time-averaged melt rates in the (a) Lagrangian and (b) Eulerian simulations in the static ice-shelf configuration. Panel (c) shows the difference between panels (a) and (b). The time averages are taken over 5 years of model time, beginning at the end of the 5 year spin up period.

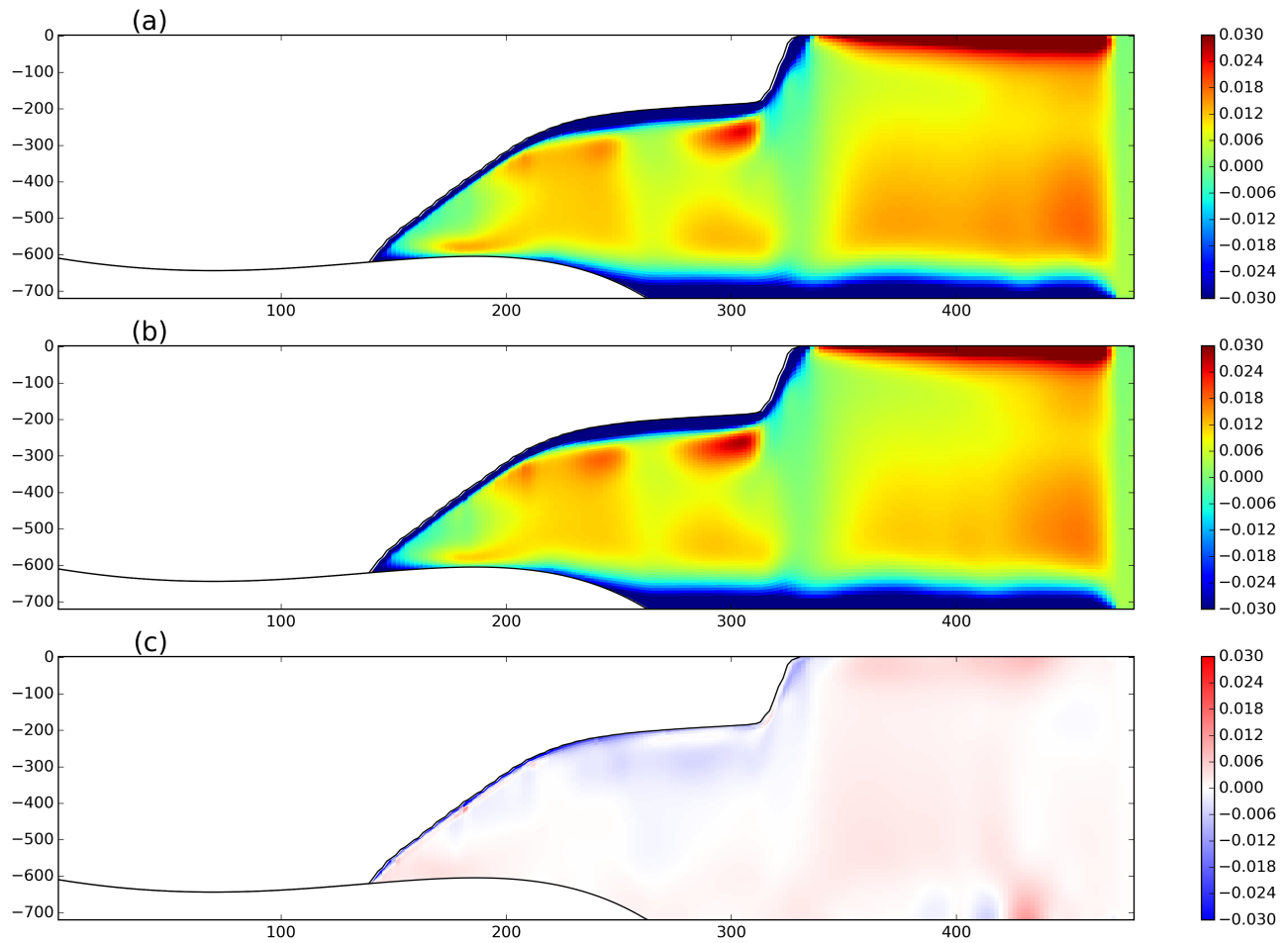


Figure S2. Time-averaged vertical sections of salinity in the (a) Lagrangian and (b) Eulerian simulations in the static ice-shelf configuration at $x=54$ km. Panel (c) shows the difference between panels (a) and (b). The time averages are taken over 5 years of model time, beginning at the end of the 5 year spin up period.